Journal of Experimental Botany, Vol. 71, No. 1 pp. 258–271, 2020
doi:10.1093/jxb/erz397 Advance Access Publication August 31, 2019
This paper is available online free of all access charges (see https://academic.oup.com/jxb/pages/openaccess for further details)

RESEARCH PAPER

Distinct metabolic pathways drive monoterpenoid biosynthesis in a natural population of *Pelargonium graveolens*

Matthew E. Bergman[1], Ángel Chávez[2], Albert Ferrer[2,3] and Michael A. Phillips[1,4,*]

[1] Department of Cellular and Systems Biology, University of Toronto, Toronto, Ontario M5S 3G5, Canada
[2] Plant Metabolism and Metabolic Engineering Program, Center for Research in Agricultural Genomics, (CRAG) (CSIC-IRTA-UAB-UB), Campus UAB, Bellaterra (Cerdanyola del Vallès), Barcelona, Spain
[3] Department of Biochemistry and Physiology, Faculty of Pharmacy and Food Sciences, University of Barcelona, Barcelona, Spain
[4] Department of Biology, University of Toronto – Mississauga, Mississauga, Ontario, L5L 1C6 Canada

* Correspondence: michaelandrew.phillips@utoronto.ca

Received 31 May 2019; Editorial decision 22 August 2019; Accepted 22 August 2019

Editor: Richard Napier, University of Warwick, UK

Abstract

***Pelargonium graveolens* is a wild predecessor to rose-scented geranium hybrids prized for their essential oils used as fragrances and flavorings. However, little is known about their biosynthesis. Here we present metabolic evidence that at least two distinct monoterpene biosynthetic pathways contribute to their volatile profiles, namely, cyclic *p*-menthanes such as (–)-isomenthone and acyclic monoterpene alcohols such as geraniol and (–)-citronellol and their derivatives (referred to here as citronelloid monoterpenes). We established their common origin via the 2*C*-methyl-D-erythritol-4-phosphate pathway but found no indication these pathways share common intermediates beyond geranyl diphosphate. Untargeted volatile profiling of 22 seed-grown *P. graveolens* lines demonstrated distinct chemotypes that preferentially accumulate (–)-isomenthone, geraniol, or (–)-citronellol along with approximately 85 minor volatile products. Whole plant $^{13}CO_2$ isotopic labeling performed under physiological conditions permitted us to measure the *in vivo* rates of monoterpenoid accumulation in these lines and quantify differences in metabolic modes between chemotypes. We further determined that *p*-menthane monoterpenoids in *Pelargonium* are likely synthesized from (+)-limonene via (+)-piperitone rather than (+)-pulegone. Exploitation of this natural population enabled a detailed dissection of the relative rates of competing *p*-menthane and citronelloid pathways in this species, providing real time rates of monoterpene accumulation in glandular trichomes.**

Keywords: Essential oils, Geraniaceae, glandular trichomes, isotopic labeling, monoterpenoid biosynthesis, untargeted metabolomics, volatile profiling.

Introduction

Scented geraniums (*Pelargonium* spp.) are an aromatic genus of glandular trichome (GT)-bearing plants in the family Geraniaceae noted for their terpenoid-rich essential oil (EO), a feature that has made them useful in the flavor, perfume, and fragrance industries. Several wild species, including *P. capitatum*, *P. graveolens*, and *P. radens*, contributed to modern cultivars as

Abbreviations: C:G, citronellol:geraniol; DMADP, dimethylallyl diphosphate; EO, essential oil; GC-MS, gas chromatography–mass spectrometry; GDP, geranyl diphosphate; GT, glandular trichomes; MEP, 2*C*-methyl-D-erythritol-4-phosphate; MVA, mevalonate; IDP, isopentenyl diphosphate.

a result of centuries of complex hybridization by European breeders using specimens collected around the Cape area of South Africa during the 18th and 19th centuries (Demarne and Van der Walt, 1989; Lis-Balchin *et al.*, 2003; Tucker and Debaggio, 2009). These scented geraniums are close relatives of the more widely cultivated regal pelargoniums (*P. domesticum*) and zonal geraniums (*P.* × *hortorum*) (Loehrlein and Craig, 2000, 2001). The term 'Graveolens cultivar group' is sometimes used to distinguish so-called rose-scented geraniums with clear *P. graveolens* heritage, but rampant hybridization has resulted in complex lineages of unclear ancestry. Commercial hybrids are widely cultivated for the perfumery, flavoring, and cosmetics industries (Blerot *et al.*, 2016), but EO from rose-scented geraniums has also attracted interest for its efficacy as an antimicrobial (Lis-Balchin and Deans, 1997; Lis-Balchin *et al.*, 1998; Nadjib Boukhatem *et al.*, 2013) and acaricidal food preservative (Jeon *et al.*, 2009), as a fumigant (Seo *et al.*, 2009; Baldin *et al.*, 2015), and for its hypoglycemic and anti-oxidant properties (Chen and Viljoen, 2010; Boukhris *et al.*, 2012, 2015).

Pelargonium EO consists primarily of oxygenated C_{10} monoterpenoid volatiles with variable amounts of C_{15} sesquiterpenes. While the monoterpenoid fraction of *Pelargonium* EO varies according to the cultivar and season (Verma *et al.*, 2013), it consists primarily of acyclic monoterpene alcohols geraniol and (−)-citronellol (and their aldehyde, acid, and ester derivatives, referred to collectively here as 'citronelloid monoterpenes'), oxygenated *p*-menthanes such as (+)-menthone and (−)-isomenthone, and lesser amounts of olefinic hydrocarbons such as limonene and β-phellandrene (Fig. 1; Babu and Kaul, 2005; Karami *et al.*, 2015; Blerot *et al.*, 2016). These volatile compounds are thought to accumulate in type 1 and 2 capitate glandular trichomes on the leaf surface (Boukhris *et al.*, 2013*a*). Phytochemical analysis has suggested the total volatile complement of *Pelargonium* consists of more than 100 compounds, the bulk of which are terpenoids (Kulkarni *et al.*, 1998; Jain *et al.*, 2001; Shellie and Marriott, 2003; Wang *et al.*, 2014).

Plant breeders have focused on cultivars rich in geraniol and (−)-citronellol as they impart a pleasing rosy fragrance (Verma *et al.*, 2013) while cultivars with a higher (−)-isomenthone content (Kulkarni *et al.*, 1998) present minty aromas with lower market value. Wild type *P. graveolens* often features abundant (−)-isomenthone (Lalli *et al.*, 2006), and breeding efforts have resulted in a shift towards strains higher in citronelloids and lower in *p*-menthane monoterpenes. A low citronellol:geraniol (C:G) ratio is an important determinant of geranium EO quality as well as an indicator of its geographical origin. This ratio varies with ambient temperature in field-grown cultivars, but the relationship is not straightforward. Warmer months favored citronellol and its esters over geraniol in the Graveolens group 'Bourbon' cultivar (Rajeswara Rao *et al.*, 1996). However, a high C:G ratio also correlates with low night-time temperatures in the 'Graveolens G1' clone (Doimo *et al.*, 1999). Interestingly, citronelloid dominant cultivars readily revert to a wild-type, isomenthone-rich phenotype as a result of somatic mutagenesis (Kulkarni *et al.*, 1998; Gupta *et al.*, 2001; Saxena *et al.*, 2004). Thus, the C:G ratio in citronelloid-rich cultivated varieties is under environmental control while the prevailing structural group (i.e. citronelloids or *p*-menthanes) is evidently controlled at the genetic level.

Essentially all monoterpenes are derived from geranyl diphosphate (GDP), itself the product of two C_5 units derived from the 2*C*-methyl-D-erythritol-4-phosphate (MEP) pathway in the plastid (Phillips *et al.*, 2008; Banerjee and Sharkey, 2014; Frank and Groll 2017). The MEP pathway synthesizes isopentenyl and dimethylallyl diphosphate (IDP and DMADP) from glyceraldehyde-3-phosphate and pyruvate in a seven-step process that in turn provides the precursors for the synthesis of primary terpenoid metabolites including chlorophyll and prenylquinones (Hoeffler *et al.*, 2002; Kim *et al.*, 2013; Liu and Lu, 2016), phytohormones (Nambara and Marion-Poll, 2005; Sakakibara, 2006; Hedden and Thomas, 2012), and carotenoids (Ruiz-Sola and Rodríguez-Concepción, 2012) in addition to a diverse suite of terpenoid secondary metabolites (Gershenzon and Dudareva, 2007). IDP and DMADP can also be formed through the cytosolic mevalonate (MVA) pathway, which utilizes acetyl-CoA as a carbon source and supplies the synthesis of mainly sesquiterpenes (C_{15}) and triterpenes (C_{30}) (Bach *et al.*, 1999). In some plant lineages, terpenoid secondary metabolism is associated with GTs. For example, the MEP pathway supplies monoterpene biosynthesis in GTs in members of the Geraniaceae (Blerot *et al.*, 2016), Cannabaceae (Booth *et al.*, 2017; Champagne and Boutry, 2017), Solanaceae (Balcke *et al.*, 2017), and Lamiaceae (McCaskill *et al.*, 1992; Hallahan, 2000).

The peppermint (*Mentha* × *piperita*) (−)-menthol pathway is currently the best characterized system for understanding monoterpene biosynthesis in GTs, an elaborate multi-step pathway spanning at least three subcellular

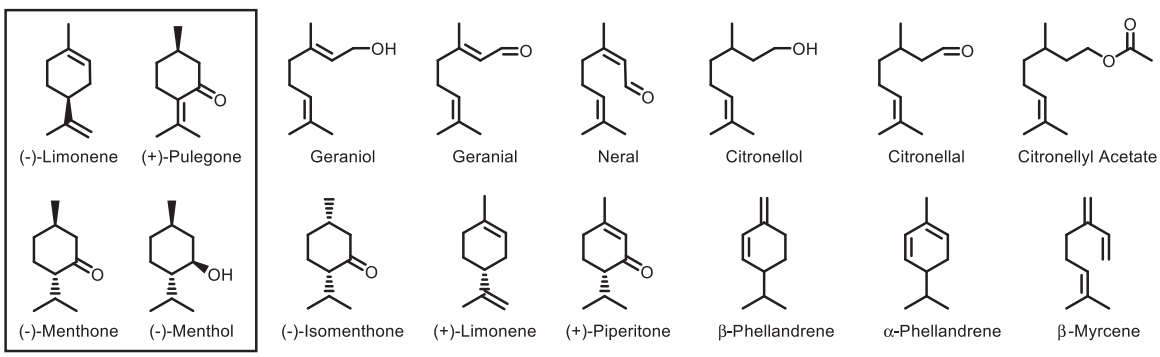

Fig. 1. Chemical structures of essential oil components commonly found in the oil of *Mentha* spp. (boxed) and *Pelargonium* spp.

compartments (reviewed in Croteau *et al*., 2005; Lange, 2015). Briefly, GDP is cyclized into (−)-limonene in the plastid by (−)-limonene synthase followed by its oxidation to (−)-*trans*-isopiperitenol in the endoplasmic reticulum by (−)-limonene-3-hydroxylase. This intermediate reaches the mitochondria where (−)-*trans*-isopiperitenol dehydrogenase oxidizes it into (−)-isopiperitenone. In the cytosol, reduction of the double bond by (−)-isopiperitonene reductase yields (+)-*cis*-isopulegone, which is then isomerized into (+)-pulegone, the penultimate precursor before (−)-menthol formation. (+)-Pulegone reduction by NADPH-dependent (+)-pulegone reductase yields (−)-menthone and lesser amounts of (+)-isomenthone. Reduction of these cycloketones to (−)-menthol and (+)-isomenthol, respectively, occurs in the cytosol, although (−)-menthol is the principal end-product.

By contrast, little is known about the biosynthesis of the corresponding compounds in *Pelargonium*. Peppermint and *Pelargonium* share two *p*-menthane cycloketones in common but the stereochemistry is inverted (*Pelargonium* accumulates (+)-menthone and (−)-isomenthone) (Ravid *et al*., 1994). Blerot *et al*. recently described four terpene synthases from *P. graveolens*, including a geraniol synthase and the sesquiterpene synthase responsible for 10-*epi*-γ-eudesmol (Blerot *et al*., 2018). The precursor to (−)-isomenthone remains unknown in *P. graveolens.* It is likewise unclear whether citronelloid and *p*-menthane monoterpenes share common biosynthetic intermediates downstream of GDP in this species or whether they constitute independent pathways competing for a common pool of GDP. Here we have applied isotopic labeling studies and untargeted metabolomic analysis to a natural population of *P. graveolens* consisting of well-defined chemotypes that preferentially accumulate geraniol, (−)-citronellol, or (−)-isomenthone. With this approach, we observed the functional independence of *p*-menthane and citronelloid monoterpene biosynthesis in closely related *P. graveolens* genetic backgrounds and inferred previously unknown features of this biosynthetic network. For instance, unlike the related (−)-menthol pathway in peppermint, we present evidence that *P. graveolens p*-menthane biosynthesis utilizes (+)-piperitone as a biosynthetic intermediate in place of (+)-pulegone and uses (+)-limonene as a precursor.

Materials and methods

Unless otherwise specified, all chemical reagents and solvents were purchased from Sigma Aldrich Canada Ltd.

Plant materials and growth conditions

Wild-type *P. graveolens* seeds, *P. tomentosum*, and the 'Attar of Roses', 'Mabel Grey', and 'Graveolens' cultivars were obtained from Fibrex Nurseries, Ltd (Stratford-Upon-Avon, UK). *Pelargonium radens*, *P. scabrum*, *P. denticulatum*, *P.* × *fragrans*, *P. grossularioides*, and the 'Orange Fizz', 'Coconut', 'Nutmeg', 'Apple', and 'Almond' scented geranium cultivars were purchased from Richter's Herbs (Goodwood, Canada). Wild-type *P. graveolens* seeds were germinated in BX M soil (ProMix, Rivière-du-Loup, Canada) supplemented with vermiculite under greenhouse conditions at 21 °C with natural lighting. A total of 22 wild-type seed-grown *P. graveolens* individuals were obtained. All plant lines were propagated by cuttings at 6-week intervals and grown at 24–26 °C under neutral photoperiod with natural and supplemental lighting in the range of 200–400 μmol photons m^{-1} s^{-1} (or photosynthetically activate radiation, PAR). Night-time temperatures ranged from 18–20 °C. All-purpose Miracle Gro (NPK 24-8-16) was applied once per week.

Whole plant isotopic labeling

Approximately 3 weeks after rooting, potted 'Graveolens' cultivar or *P. graveolens* wild-type lines were labeled in a dynamic flow cuvette under physiological conditions. Cuttings were rooted in 250 ml pots in BX soil mix and grown in the greenhouse for a further 3–4 weeks prior to use in labeling experiments. Labeling experiments were conducted in a custom-built 2-liter dynamic flow cuvette into which four individual potted plants fit. Air flow was maintained at 1.0 l min^{-1} using a pressurized air tank containing normal air (400 μl l^{-1} CO_2) for approximately 45 min, during which time gas exchange measurements were made with a Li-Cor 840a (Lincoln, NE, USA) CO_2/H_2O gas analyser connected to the cuvette exhaust. Light intensity, as judged by a Li-Cor 250A quantum meter, was maintained at 250 PAR using a custom light bank consisting of Cree XPE high intensity white LEDs equipped with a potentiometer and high-capacity cooling fan (LEDMania, Barcelona, Spain). A mixing fan inside the cuvette ensured proper mixing of air within the chamber. The humidity was maintained at approximately 70% by passing the air through a wash bottle chilled in an ice bath, and the internal cuvette temperature was kept between 24 and 26 °C based on thermometer readings. Once gas exchange readings indicated a near photosynthetic steady state as inferred by less than 5% variation in CO_2 assimilation over 5 min (generally 45–60 min), the air source was switched to an alternative air tank in which the CO_2 was 99% enriched by $^{13}CO_2$ at the same concentration of 400 μl l^{-1} CO_2 (Linde Canada, Ltd, Mississauga, Ontario, Canada). The decay of the $^{12}CO_2$ signal as detected by the inline infrared gas analyser was used to calculate the half-life of the atmospheric exchange. Labeling times were corrected to the halfway point during introduction of the labeling atmosphere into the flow cuvette. Groups of four plants were labeled from 3 to 9 h at 1 h intervals. Four biological replicates were used for each time point for time course series. At the end of labeling experiments, 50 mg of tissue from the youngest two leaves was harvested by vortexing in 500 μl ethyl acetate containing internal standards as described below. Labeling experiments were conducted between 10.00 and 14.00 h to minimize diurnal effects, except where longer labeling experiments precluded this. In that case, experiments were performed from 09.00 until 18.00 h for the longest time points.

Inhibitor treatments

For exogenous treatments, plants were sprayed at 1, 2, and 3 d before labeling. Inhibitor treatments consisted of spraying with one of the following: 150 μM clomazone, 250 μM mevinolin (all in 1% (v/v) dimethylsulfoxide (DMSO)), or 1% DMSO only (negative controls)). Inhibitor-treated plants were labeled using a single time point of 6 h. For a given labeling experiment of inhibitor-treated plants, one plant from each inhibitor group and the negative control group were each included. These experiments were carried out over 8 d for a total of five replicates.

Harvest and extraction of plant tissues

Extracts of volatile compounds were obtained from 50 mg fresh leaf tissue (labeled or unlabeled) steeped overnight at −20 °C in 500 μl HPLC-grade ethyl acetate (Caledon Laboratory Chemicals) in a 5 ml round-bottom screw-cap glass extraction vial (Fisher Scientific) along with 3,7-dimethyl-1-octanol at 50 μg ml^{-1} as internal standard. The following day, extraction vials were vortexed at room temperature for 40 min then purified over a 0.8 ml glass column containing equal parts silica gel (60 Å, 60–100 mesh) and anhydrous $MgSO_4$. The column was pre-washed with 400 μl ethyl acetate. The sample was applied to the column and eluted with an additional 200 μl ethyl acetate. Extracts were shielded from light and stored at 4 °C under seal until analysed by gas chromatography–mass spectrometry (GC-MS). Each wild-type line was sampled and extracted on three separate occasions.

Volatile analysis by GC-MS

Plant volatiles were analysed as organic extracts; 1 µl purified ethyl acetate extracts of plants tissue was analysed on an Agilent Technologies® 7890B GC system coupled to a 5977C mass selective detector utilizing electron impact ionization at 70 eV (positive mode). Extracts were analysed on the following stationary phases: an HP-5ms capillary column (30 m length, 0.25 mm i.d., 0.25 µm film thickness; Agilent Technologies), an HP-Innowax (30 m length, 0.25 mm i.d., 0.15 µm film thickness; Agilent Technologies), and a Cyclodex-B column (30 m length, 0.25 mm i.d., 0.25 µm film thickness; Agilent Technologies). The HP-5ms column was used for *P. graveolens* chemotype volatile profiling, while the Innowax column was used for label incorporation studies and the β-cyclodex column was used for chiral GC-MS analysis of limonene enantiomers. For analysis on the HP-5ms column, 1 µl extract was injected in split mode (1:20) with the injection port set to 225 °C. The oven conditions were as follows: 70 °C for 2 min then increasing at 0.7 °C min^{-1} to 100 °C and held for 3 min, 50 °C min^{-1} to 280 °C, with a 5 min final hold time. For analysis on the Innowax column, 1 µl extract was injected in split mode (1:50) with the injection port set to 225 °C. The oven conditions were as follows: 40 °C for 4 min then increasing at 3 °C min^{-1} to 170 °C, 50 °C min^{-1} to 260 °C with a 5 min final hold time. Lastly, for the β-cyclodex column, 1 µl extract was injected in split mode (1:20) with the injection port set to 250 °C. The oven conditions were as follows: 70 °C for 20 min then increasing at 10 °C min^{-1} to 210 °C with a 5 min final hold time. For solid phase microextraction (SPME)-based injections, 100 mg fresh tissue was enclosed in a headspace vial and incubated with an exposed polydimethylsiloxane fiber at 22 °C for 60 s and then injected manually with all other settings as above.

Mass data were collected according to two acquisition regimes. First, data were acquired in scan mode (m/z 50–225) with a scan rate of 5 Hz. Second, labeled tissue extracts were re-analysed using a selected ion mode (SIM) method that detects exclusively the molecular ion and ^{13}C-labeled isotopologs of prominent volatile compounds. To accomplish this, multiple scheduled SIM windows were implemented to monitor label incorporation in the molecular ion cluster for compound classes of similar masses as follows: olefinic monoterpenes, m/z 136–146 at 30 ms for each mass unit, followed by oxygenated monoterpenes, m/z 152–166 at 21 ms per mass unit; and select sesquiterpenes, m/z 204–214, coupled with monoterpene ester components at m/z 154–164 at 15 ms per mass unit. For chiral GC-MS analysis of labelled samples, three SIM windows were used: olefinic monoterpenes, m/z 136–146 at 25 ms per mass unit; oxygenated monoterpenes, m/z 152–164 with m/z 57 and 70 for internal standards at 19 ms per mass unit; and the final window for esters and sesquiterpenes, m/z 152–164, 204–206 at 18 ms per mass unit.

Data analysis

For the analysis of GC-MS volatile data, peak integration of total ion chromatograms and extraction of mass spectra were accomplished using the Agilent MassHunter workstation (version B.07 service pack 2). Identification of features was carried out in MassHunter Qualitative Analysis based on spectral matches to the NIST2014 mass spectral library and comparison with the literature (Kulkarni *et al.*, 1998; Jain *et al.*, 2001; Shellie and Marriott, 2003; Wang *et al.*, 2014). All identifications were confirmed by matching retention times and mass spectra to those of in-house authentic standards except where indicated. For untargeted profiling, spectral deconvolution, peak picking, and alignment were performed using multiple independent approaches. First, raw data were deconvoluted and aligned with MassHunter Profinder (version B.08) using the top 132 volatile features reproducibly detected in 177 biological replicates of cultivars and wild-type *P. graveolens* lines. In parallel, a Python script was developed to facilitate peak picking from integrated peak data obtained in MassHunter Qualitative Analysis. Feature matching was ensured by base peak and retention index alignment. Principal component analysis, hierarchical clustering, and correlation analysis of all GC-MS data were carried out using the Metaboanalyst online suite of metabolomics analysis tools (Xia *et al.*, 2015; Chong *et al.*, 2018) and standard R packages (Galili, 2015; Wickham, 2016; Galili *et al.*, 2017). Absolute quantification was performed by linear regression to individual external standard curves constructed from authentic standards and corrected for recovery of the internal standard.

Results and discussion

Volatile profiling in a P. graveolens *natural population suggests mutually exclusive* p*-menthane and citronelloid specialists*

We compared the volatile profiles of 22 seed-grown individuals from a wild population of *P. graveolens* to identify possible chemotypes. GC-MS analysis of *P. graveolens* volatiles was carried out on trichome-rich, expanding leaf tissue. Untargeted profiling identified a total of 322 volatile features among all lines. From this group, 89 were reproducibly detected within the individual plant lines. Principal component analysis of the 22 lines was carried out using these 89 volatile compounds as input variables (Fig. 2). Approximately 77% of the variation was explained by the first component, while the second accounted for another 20%. Lines positively correlated with the first component were highly enriched in the *p*-menthane monoterpene (−)-isomenthone (15 lines), while lines correlated negatively with the first component demonstrated enrichment with citronelloid monoterpenes such as geraniol (two lines), and (−)-citronellol (five lines). Thus, the single most defining factor in the volatile profile of a given line was whether it was dominated by cyclic *p*-menthane type or acyclic citronelloid type monoterpenes. *Pelargonium graveolens* lines enriched in the citronelloid monoterpenes geraniol and (−)-citronellol (and, to a lesser extent, (−)-citronellal) varied principally along the

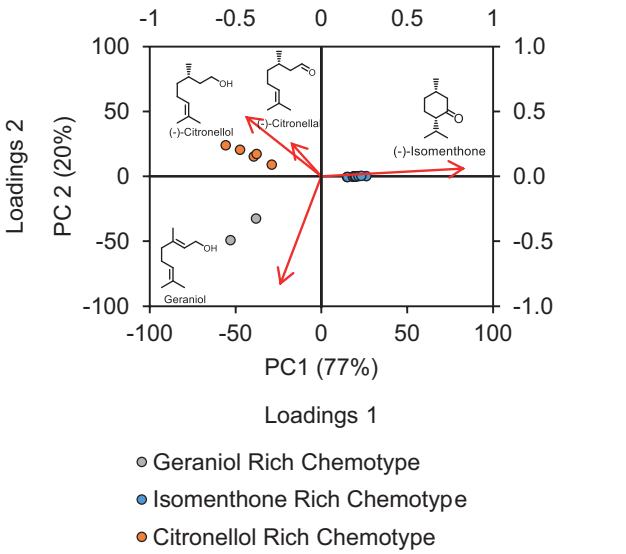

Fig. 2. Mixed score and loading plot derived from principal component analysis of wild-type *P. graveolens* volatile profiles. Eighty-nine variables representing EO features (mainly monoterpenoids and a limited number of sesquiterpenes) were compared among 22 genetically distinct groups representing independent seed-grown lines. Ethyl acetate extracts were obtained from multiple cuttings from each line (n=4–6) made at different times of the year. The first two components explain 77% and 20% of the variation, respectively. Chemical structures indicate the key volatile features most associated with each group: (–)-isomenthone (15 lines), (–)-citronellol (five lines, including one with high (–)-citronellal content), and geraniol (two lines). (This figure is available in color at *JXB* online.)

second component (i.e. they could be distinguished by their C:G ratios). No plant line was observed that contained equal proportions of *p*-menthane and citronelloid monoterpenes. These four volatile compounds account for most of the differences among the volatile profiles of these lines (Fig. 2). The single citronellic acid enriched line, Pg28, differed from the other four lines comprising the (−)-citronellol clade in that it lacked the aldehyde form, citronellal, but instead presented a significant level of the corresponding acid. A typical chromatogram of an (−)-isomenthone-rich line showed that upwards of 72.2% (±3.7%) of the total integrated peak area was due to this compound (Fig. 3), corresponding to an absolute concentration of 11.11±0.91 mg g^{-1} FW, followed by trace levels of other volatiles, most prominently β-myrcene and trans-β-ocimene, which made up 3.7±1.6% and 2.6±0.8% of the total integrated peak area, respectively. (−)-Citronellol-rich lines displayed greater diversity, with (−)-citronellol comprising 35.1±12.0% of the total peak area (corresponding to 5.02±0.37 mg g^{-1} FW), (−)-isomenthone 21.0±5.7%, and the remainder contributed by multiple minor components, of which (−)-citronellal and geranial contributed the largest amount by peak area at 16.1±7.2% and 1.7±1.2%, respectively (Fig. 3). Finally, the profiles of members of the geraniol-rich group consisted of approximately 50.5±12.0% geraniol (4.76±0.96 mg g^{-1} FW), followed by 15.4±10.4% (−)-isomenthone and 11.4±3.3% (−)-citronellol as its major components (Fig. 3). For comparative purposes, the 'Graveolens' cultivar, derived largely from *P. graveolens* as well as *P. radens* and *P. capitatum*, was similarly analysed and found, unlike the natural chemotypes, to contain more balanced levels of *p*-menthane and citronelloid monoterpenes. Comprehensive lists of volatile compounds in *P. graveolens* and its cultivars have been published previously (Kulkarni *et al*., 1998; Jain *et al*., 2001; Shellie and Marriott, 2003; Wang *et al*., 2014) and reviewed (Blerot *et al*., 2016). While our results are in general agreement with these volatile profiles, we have chosen to focus on the approximately six to eight volatile compounds that define differences between chemotypes and typically make up >95% of the total ion chromatogram by peak area.

When hierarchical clustering was applied to these same data, the separation of (−)-isomenthone-, geraniol-, and (−)-citronellol-rich chemotypes was evident, with 15 of the 22 lines falling into the (−)-isomenthone-rich category and five into the (−)-citronellol group (Fig. 4A). In this case, the Pg28 line clustered as a singleton within the (−)-citronellol group, while all other clusters consisted of at least two independent lines. The remaining two lines contained geraniol as their principal volatile compound. These groupings matched our principal component analysis data that showed only three to four volatile compounds were responsible for ~97% of the variation in the dataset. The (−)-isomenthone cluster could be subdivided further, mainly due to small differences in low abundance sesquiterpenes and olefinic monoterpenes. However, the cluster height of these relationships in the dendrogram did not justify further division into smaller clusters. The entire analysis was repeated approximately 6 months later to determine if seasonal or other environmental factors played a role in the observed volatile profiles. However, the relative enrichments and overall compositions were essentially identical across all seed-grown lines surveyed. From these observations, we conclude that *P. graveolens* natural populations

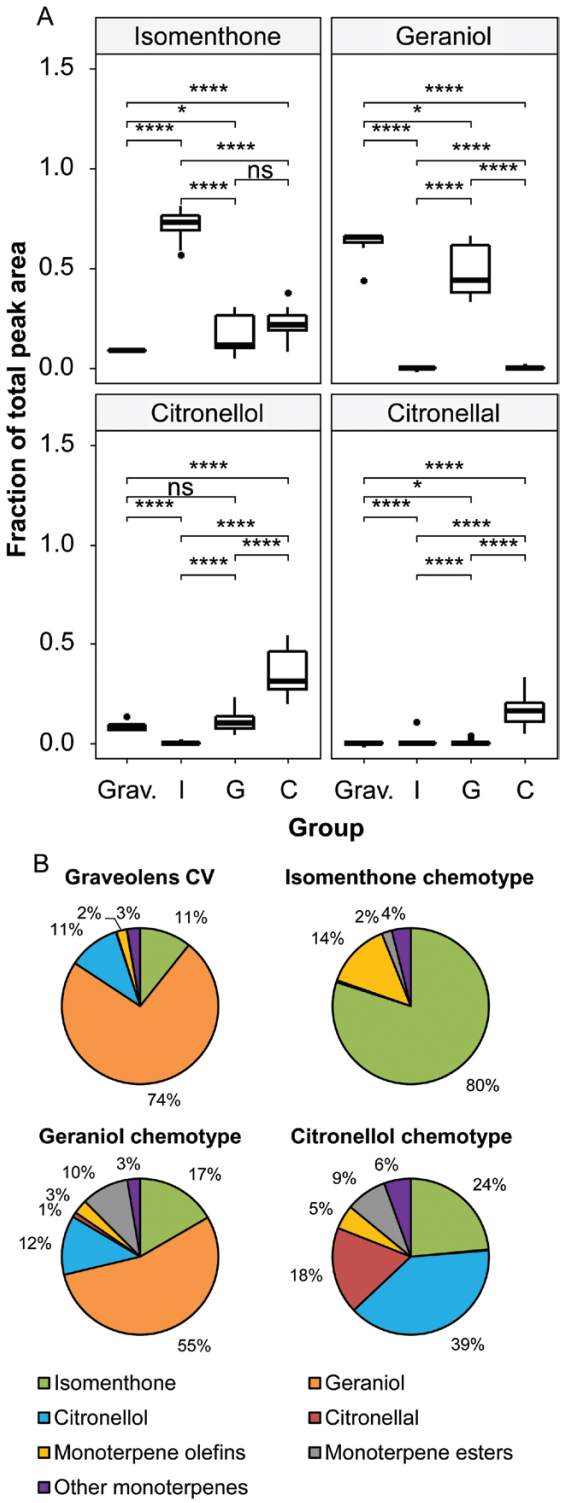

Fig. 3. (A) Principal monoterpene volatile composition associated with *P. graveolens* chemotypes by fractional peak area. (B) Summary of data shown in (A) as pie charts showing the mean proportion of key components in the volatile fraction of each chemotype. The fractional peak areas for each sample within a chemotype were included in this analysis (n=6–18 per line, 204 total). *P*-values are based on Student's two-tailed *t*-test: ns, ≥0.05; *P<0.05; ****P<0.0001. (This figure is available in color at *JXB* online.)

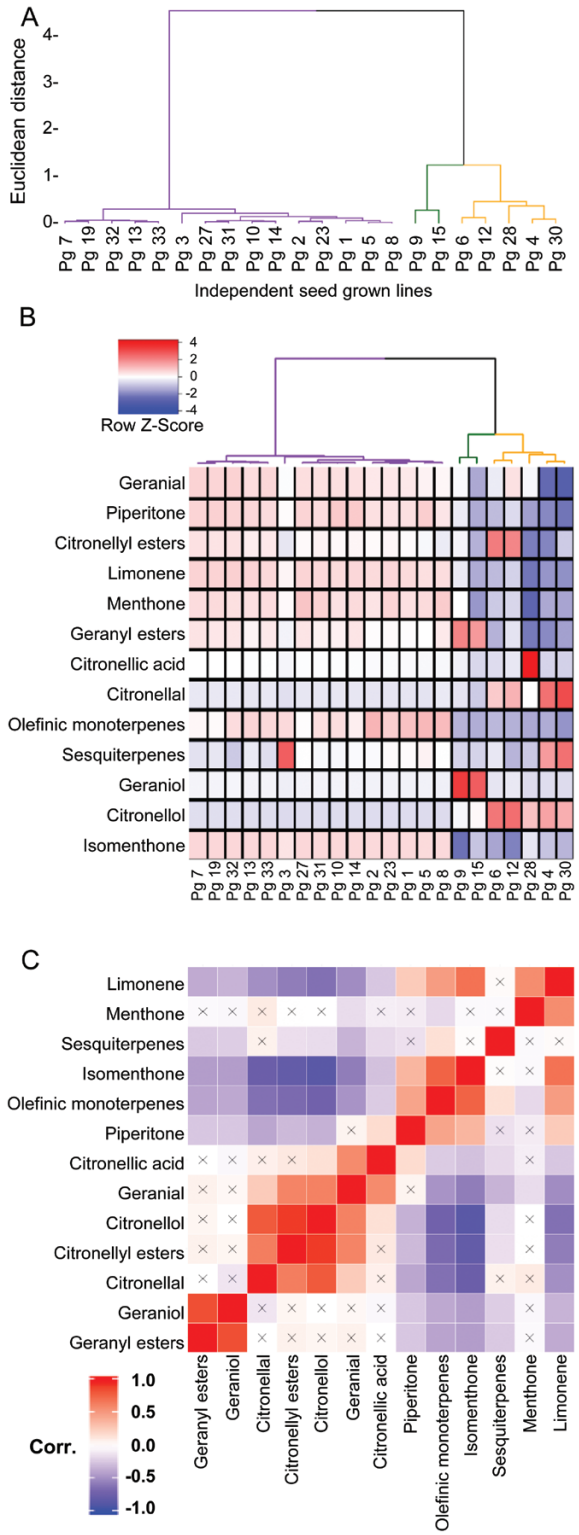

Fig. 4. (A) Hierarchical clustering of 22 *P. graveolens* wild-type lines based on volatile profiles consisting of 89 features from untargeted GC-MS analysis. All but 37 of these features corresponded to monoterpenoids. Clustering was performed using the Ward algorithm and separated by Euclidean distance. (B) Heatmap of the 13 most significant volatile features used in the hierarchical clustering of *P. graveolens* lines. (C) Corresponding correlation matrix of the same features using 204 total samples across all 22 lines based on their Pearson correlation coefficients. At least three distinct chemotypes could be distinguished based primarily on the abundance of *p*-menthane and citronelloid monoterpenes. An '×' signifies no statistically significant correlation. (This figure is available in color at *JXB* online.)

consist of phenotypes characterized by a consistent volatile chemical profile that is stable across phenological variation and generation. Furthermore, these chemotypes are dominated either by the *p*-menthane monoterpene (−)-isomenthone or by one of the citronelloid monoterpene alcohols (geraniol or (−)-citronellol). An inspection of the gross characteristics of these chemotypes did not reveal obvious differences in leaf morphology (Supplementary Fig.1 at *JXB* online). Breeding efforts that have produced commercially important varieties such as 'Algerian', 'Bourbon', and 'Kelkar' have focused on lines enriched in citronelloid monoterpenes, and genotypic variation in the relative amounts of their acyclic monoterpene alcohols is well established (Rajeswara Rao, 2009). However, our results demonstrate that the parental lines themselves that gave rise to modern rose-scented geranium cultivars featured distinct chemotypic groups that can be distinguished, firstly, by the presence or absence of (−)-isomenthone as the dominant volatile component and, secondly, for citronelloid-rich lines, by their C:G ratios. The absence of any line with comparable levels of *p*-menthane and citronelloid monoterpenes suggests that in wild-type plants, one pathway tends to predominate. We only observed comparable levels of *p*-menthane and citronelloid monoterpenes in the 'Graveolens' cultivar hybrid line.

We next examined correlations between principle volatile components and the 22 wild-type lines to infer details about their biosynthetic relationships. The heatmap in Fig. 4B indicates that in addition to the expected high abundance of (−)-isomenthone, members of the (−)-isomenthone clade also displayed higher levels of other *p*-menthane monoterpenes including limonene, (+)-menthone, and (+)-piperitone as well as a near complete absence of (−)-citronellol and geraniol. The geraniol-rich clade demonstrated a corresponding reduction in the cyclic *p*-menthanes limonene, (+)-menthone, and (−)-isomenthone as well as a high degree of enrichment of geranyl esters (principally formate, acetate, and tiglate) (Fig. 4B). Finally, the corresponding citronellyl esters were highly enriched in the (−)-citronellol clade, analogous to those observed in the geraniol group, and this clade was also characterized by an absence of *p*-menthane type monoterpenes and variable levels of (−)-citronellal.

A correlation matrix generated from these data (Fig. 4C) demonstrated the co-occurrence of several groups of monoterpene volatiles according to their structural class, suggestive of membership in a common biosynthetic sequence. For instance, the *p*-menthane monoterpenes limonene, menthone, isomenthone, and piperitone (Fig. 1) all showed a strong correlation (Pearson's correlation coefficient >0.5). Similarly, citronelloid monoterpenes including geraniol, (−)-citronellol, geranial, (−)-citronellal, citronellic acid, and citronellyl and geranyl esters showed a strong correlation to other acyclic monoterpenes (Fig. 4C). At the same time, *p*-menthane-rich lines showed a strong negative correlation (Pearson's correlation coefficient <−0.5) with citronelloids and vice versa. The positive correlation between limonene and (−)-isomenthone suggests the former may serve as precursor for *p*-menthane biosynthesis in *Pelargonium*, in keeping with a similar role for limonene as a precursor for *p*-menthane biosynthesis in the peppermint (−)-menthol pathway (Lange, 2015). The structural

similarity of piperitone to isomenthone (Fig. 1), along with the strong co-occurrence observed in this analysis, are suggestive of a precursor–product relationship. At the same time, the strong negative correlation between citronelloids and *p*-menthane in these wild-type lines indicates these two metabolic specializations may be largely mutually exclusive in natural populations.

Inhibitor treatments confirm the MEP pathway supplies monoterpene biosynthesis in Pelargonium

To determine the principal precursor pathway responsible for providing isoprene equivalents for monoterpene biosynthesis in *P. graveolens*, 'Graveolens' cultivar plants were sprayed once per day with an inhibitor of the chloroplast localized MEP pathway (clomazone, which is converted *in planta* to ketoclomazone, a potent inhibitor of 1-deoxyxylulose-5-phosphate synthase, the first enzyme in the MEP pathway; Matsue *et al*., 2006), mevinolin, which inhibits the HMG-CoA reductase step of the MVA pathway (Alberts *et al*., 1980), or a control solution. The rate of synthesis of plastid-derived terpenes, as judged by ^{13}C incorporation, should be reduced following clomazone treatment, whereas cytosolic terpenes derived from the MVA pathway should be affected by mevinolin treatment. After 72 h of inhibitor or control treatment, plants were subjected to $^{13}CO_2$ isotopic labeling assays as described above and harvested at a single time point of 6 h. We observed decreases in the rate of incorporation of ^{13}C into monoterpenoid end-product pools when plants were sprayed with clomazone (Fig. 5), but not when treated with mevinolin or a control solution. From these observations, we conclude that the MEP pathway supplies precursors for monoterpene biosynthesis in *P. graveolens*.

Isotopic labeling studies in intact plants reveal physiological rates of monoterpenoid volatile accumulation in P. graveolens

We carried out $^{13}CO_2$ labeling assays on intact plants to measure the rate of ^{13}C incorporation into various monoterpenoid volatile components and to gain insight into their biosynthetic relationships. Identical 4- to 6-month-old rooted cuttings of the 'Graveolens' cultivar were incubated in air containing $^{13}CO_2$ at 400 p.p.m. for 1–9 h following a 1 h adaptation phase in standard air in an environmentally controlled dynamic flow cuvette. Analysis of the resulting labeled organic extracts by GC-MS showed detectable levels of ^{13}C in major oil components of the 'Graveolens' cultivar such as geraniol, (−)-isomenthone, limonene, and (+)-piperitone in as little as 3 h (Fig. 6). Volatile components showing detectable label incorporation on this time scale were selected for closer analysis. Using an optimized GC-MS SIM method, we calculated the fractional labeling of each feature at each labeling time point between 0 and 9 h using the relative *m*/z intensities of the molecular ion cluster representing the unlabeled monoisotopic peak (M+0) and various isotopologs of each C_{10} volatile compound (M+1 through M+8; ions corresponding to M+9 and M+10 could not be reliably quantified with this method). These data were then compared with the absolute concentration as judged by comparison with external calibration curves.

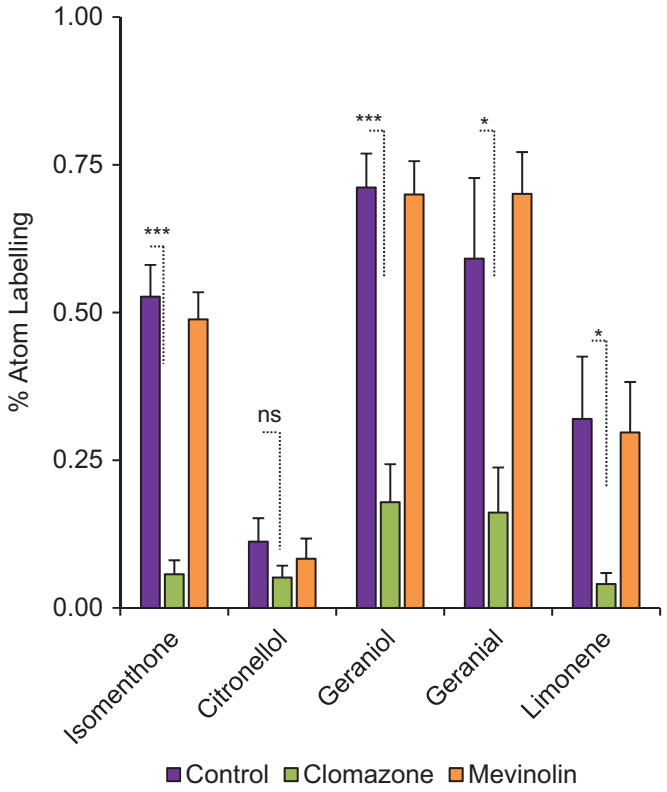

Fig. 5. Effect of inhibitor treatment on ^{13}C label incorporation into monoterpenoid pools. The 'Graveolens' cultivated variety, a hybrid that presents a mixed volatile profile consisting of the principal volatiles of the (–)-isomenthone-, (–)-citronellol-, and geraniol-rich wild-type lines, was treated with clomazone (a MEP pathway inhibitor), mevinolin (a MVA pathway inhibitor), or a control solution for 3 d and then subjected to whole plant $^{13}CO_2$ labeling assays. Volatile terpenes were extracted following 6 h whole-plant labelling. Percentage atom labeling was calculated by subtracting natural isotopic abundance values obtained from unlabeled control samples. Significant differences were inferred through a two-tailed Student's *t*-test (n=5). *P*-values are as follows: ns, ≥0.05; *P<0.05; ***P<0.001. (This figure is available in color at *JXB* online.)

The combined data allowed us to express the moles of ^{13}C equivalents detected in each metabolite pool over time.

This whole plant isotopic labeling approach permitted us to measure the rate of monoterpenoid accumulation in glandular trichomes under physiological conditions in intact plants. The volatile profile of the 'Graveolens' cultivar consists of significant amounts of geraniol, (−)-citronellol, and (−)-isomenthone (Fig. 3) and thus provides a useful starting point to collectively evaluate the relative rates of the three major end-products in a single plant line. We observed the highest rate of label incorporation into geraniol and (−)-isomenthone in this line, which became labeled at a rate of 278 and 250 pmol ^{13}C mg^{-1} FW h^{-1}, respectively (Fig. 6). This rapid rate of labeling would be consistent with a direct formation of geraniol from GDP. However, a comparable rate of label incorporation into (−)-isomenthone, which is expected to undergo a longer series of transformations from GDP, was unexpected. (−)-Citronellol and (+)-piperitone both showed significantly lower rates of incorporation in this hybrid line at 56 and 65 pmol ^{13}C mg^{-1} FW h^{-1}, respectively, but the lowest incorporation rate was observed for limonene at only 29 pmol ^{13}C mg^{-1} FW h^{-1}.

We then applied this whole plant time course labeling approach to plants representing the three major chemotypes to observe the synthesis of *p*-menthane and citronelloid monoterpenes in isolation. To do this, we relied on a β-cyclodextrin capillary GC column that is capable of resolving simple enantiomeric pairs. It should be noted that due to improvements in growth and labeling conditions used in wild-type labeling assays, these results cannot be directly compared with those of the 'Graveolens' cultivar. Differences in flux towards *p*-menthane and citronelloid monoterpenes were readily observed among the three main chemotypes (Table 1). For instance, in *p*-menthane ((−)-isomenthone)-enriched chemotypes, ^{13}C label appeared in the (−)-isomenthone pool beginning at 3 h and increased at a rate of 1719 pmol ^{13}C mg^{-1} FW h^{-1} (Supplementary Fig. S2), whereas the flux of ^{13}C into (−)-isomenthone in the citronellol- and geraniol-rich chemotype was only 218 and 70 pmol ^{13}C mg^{-1} FW h^{-1}, respectively. In contrast, label appeared above background levels in only 2 h in the geraniol pool of the geraniol-rich chemotype, increasing at a rate of 381 pmol ^{13}C mg^{-1} FW h^{-1} (and undetectable in (−)-citronellol- and (−)-isomenthone-rich lines).

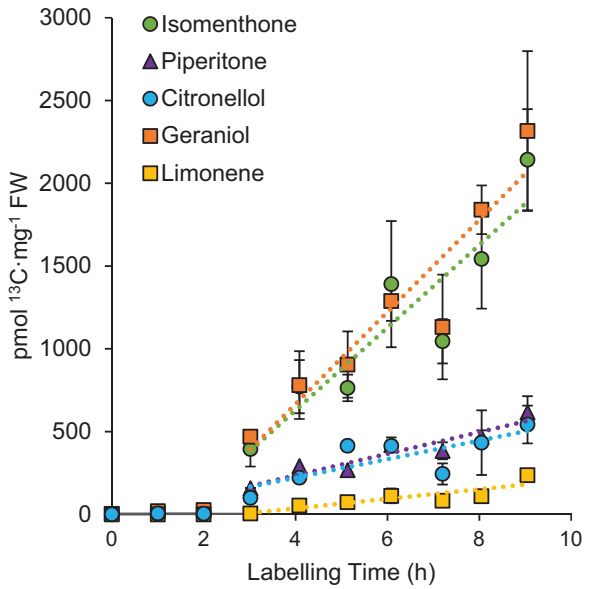

Fig. 6. Time course labeling of monoterpenoid pools in the 'Graveolens' cultivar. Plants were equilibrated under a normal atmosphere consisting of 400 ppm CO_2 until gas exchange measurements indicated a photosynthetic steady state, then labeled with 400 ppm $^{13}CO_2$ for 3–8 h prior to harvest and extraction. Absolute label incorporation was calculated as the product of the fractional labeling of the metabolite pool and absolute concentration as inferred by internal standard-normalized external calibration curves established for each analyte. For comparative purposes, all labeling values were converted to pmol of ^{13}C equivalents. Linear regressions of the resulting incorporation curves are as follows: geraniol, $y=278x-51$ ($R^2=0.892$); (–)-isomenthone, $y=249x-35$ ($R^2=0.848$); (–)-citronellol, $y=56x-2.58$ ($R^2=0.625$); (+)-piperitone, $y=65x-26$ ($R^2=0.895$); limonene: $29x-79$ ($R^2=0.757$). Error bars signify the standard error of four biological replicates. (This figure is available in color at *JXB* online.)

Quantification of other *p*-menthane intermediates in the (−)-isomenthone-rich strain was also feasible with this approach. Increases in label were detected in (+)- and (−)-limonene at rates of 72 and 13 pmol ^{13}C mg^{-1} FW h^{-1}, respectively, while (+)-piperitone labeling was observed at a rate of 849 pmol ^{13}C mg^{-1} FW h^{-1}. Geraniol was present only at trace levels in this chemotype, and ^{13}C label in this metabolite pool was indistinguishable from background levels. These observations, together with correlation data (Fig. 4), lead us to conclude that *p*-menthane and citronelloid biosynthesis operate independently, rely on the same GDP precursor pool, and do not appear to share any downstream intermediates.

These direct metabolic data impact our understanding of how essential oil biosynthesis takes place in *P. graveolens*, although the interpretation is not straightforward. If limonene serves as precursor to (−)-isomenthone via (+)-piperitone, our initial expectation was that upstream intermediates should show an incorporation rate at least as high as downstream intermediates in order to sustain the needed supply. That this was not the case may be explained by several possibilities. Firstly, the precursor for (−)-isomenthone might be something other than limonene, despite strong correlation and heatmap data that suggest their membership in a common biosynthetic sequence. However, the observed labeling patterns may also be explained by significant back reactions for reversible steps, significant departure

Table 1. *Rates of ^{13}C label incorporation into monoterpenes for three* P. graveolens *chemotypes, as judged by linear regression of time course labeling assays*

	(–)-Limonene	(+)-Limonene	Isomenthone	Citronellol	Piperitone	Geraniol	Citronellal
Citronellol chemotype							
Slope[a]	0	0	217.93	465.01	136.47	0	242.03
Intercept[b]	0	0	–368.63	–436.01	–143.56	0	–308.15
R^2	0	0	0.805	0.761	0.712	0	0.746
Geraniol chemotype							
Slope[a]	0.11	3.50	69.68	1.69	0	380.83	0
Intercept[b]	0.78	–7.35	409.91	–2.97	0	515.28	0
R^2	0.035	0.505	0.082	0.091	0	0.130	0
Isomenthone chemotype							
Slope[a]	12.88	71.94	1719	0	848.96	0	0
Intercept[b]	–26.2	–158.2	–3700	0	1849.2	0	0
R^2	0.871	0.955	0.965	0	0.939	0	0

[a] pmol ^{13}C mg^{-1} FW h^{-1}.
[b] pmol ^{13}C mg^{-1} FW.

from true steady state conditions, or long-range transport of certain intermediates as glycosides (Wüst *et al*., 1999) and their subsequent deconjugation. Moreover, multiple transport processes, cell types, and central metabolic pathways are involved in the biosynthesis of these labeled natural products that together could introduce unpredictable effects on label distribution. These include the fixation of $^{13}CO_2$ in photosynthetic cells via the Calvin–Benson cycle, conversion to sucrose or other sugars, transport to the leucoplasts of glandular trichomes (Turner *et al*., 1999), partial degradation via glycolysis to form pyruvate and glyceraldehyde 3-phosphate, conversion to IDP and DMADP through the MEP pathway, assembly of GDP, and then as of yet uncharacterized steps culminating in the formation of labeled monoterpenoid end-products. Unequal loss of some intermediates through volatilization may further skew these results. The transport to the subcuticular storage space of captitate glandular trichomes (Tissier *et al*., 2017) represents an additional step that may complicate monoterpenoid labeling, although our analytical system does not distinguish between intercellular labeled monoterpenes awaiting transport and those in the storage cavity. Finally, glycosylation and transport of some intermediates may partly contribute to these observations. While little is known regarding terpene glycoside formation in *P. graveolens* compared with the glycosylation of flavonoids (Boukhris *et al*., 2013*b*), conjugation of terpene alcohols to sugar residues is well known in other plant systems (Houshyani *et al*., 2013; Andrade *et al*., 2018). Future studies taking conjugation into account and diversion of photosynthate into sequestered glycoside pools will be necessary to build comprehensive models for the biosynthesis of these metabolites.

Despite the inconsistencies in precursor–product labeling patterns in limited cases, these results overall provide useful insights into the kinetics of multiple processes linking primary and secondary metabolism. For example, we have shown that ^{13}C label, starting from $^{13}CO_2$, is detectable in functionalized monoterpenoid end-products such as (−)-isomenthone in as little as ~2 h in illuminated plants, and less for geraniol. Previous reports of $^{13}CO_2$ whole plant volatile labeling have focused on emitted monoterpenes in herbivory-stressed cotton (Pare and Tumlinson, 1997) or oak (Loreto *et al*., 1996), or isoprene emissions in oak and poplar (Delwiche and Sharkey, 1993; Karl *et al*., 2002; Loreto *et al*., 2004; Ghirardo *et al*., 2014). However, the present report may constitute the first direct kinetic assessment of carbon flux into stored monoterpenoids in the GTs of intact plants.

(+)-Limonene is the likely precursor to the p*-menthane monoterpene biosynthesis* Pelargonium

The asymmetrical incorporation patterns of (+)- and (−)-limonene in the (−)-isomenthone chemotype (Table 1) led us to further investigate the precursor to (−)-isomenthone. Unlike peppermint, which accumulates almost exclusively (−)-limonene as a precursor to (−)-menthol biosynthesis, or lemon grass (*Cymbopogon citratus*), which accumulates mostly the (+) enantiomer, *P. graveolens* EO from the two citronelloid chemotypes features a nearly racemic mixture of the (+) and (−) forms of limonene (Fig. 7A). In the case of the (−)-isomenthone chemotype, this ratio is skewed towards (+)-limonene (63%). Most plant species typically favor one enantiomer over the other in the case of chiral natural products. However, exceptions to the rule exist. Pine produces significant quantities of (+)- and (−)-α-pinene (Phillips *et al*., 1999), for example. In this case, there is a dedicated terpene synthase responsible for each enantiomer (Phillips *et al*., 2003) rather than a single terpene synthase capable of producing both. Since limonene is the most abundant monoterpene hydrocarbon in *P. graveolens* and because it serves as precursor to the *p*-menthane monoterpenes in peppermint, we examined carbon flux into (+)- and (−)-limonene to determine whether the observed differences in pool size of these two enantiomers among chemotypes were paralleled by chemotypic differences in carbon flux. Percentage atom labeling analysis of the two limonene enantiomers in the (−)-isomenthone-rich lines demonstrated that 81% of the observed limonene flux goes through the (+) enantiomer (Fig. 7C). The citronelloid-rich lines demonstrated far lower levels of limonene overall, and the isotopic enrichment did not favor (+)-limonene to the extent seen in (−)-isomenthone-rich chemotypes (Fig. 7B). The absolute rate of ^{13}C incorporation into (+)-limonene (72 pmol ^{13}C mg^{-1} FW h^{-1}) in the (−)-isomenthone-rich line was >20 times the rate of flux into (+)-limonene in geraniol-rich lines, which partly reflects the smaller pool size of limonene in this line, and no flux was detected into (+)-limonene in the (−)-citronellol chemotype (Table 1). Therefore, given the correlation data above and the stereospecific incorporation of ^{13}C into (+)-limonene, a pattern specific to the (−)-isomenthone line, (+)-limonene is currently the best candidate for the precursor to (−)-isomenthone biosynthesis in *P. graveolens*. Further investigation via biochemical characterization of recombinant proteins is needed to confirm this preliminary conclusion.

Pulegone is not an intermediate of Pelargonium p*-menthane biosynthesis*

We investigated whether pulegone is an intermediate in *p*-menthane biosynthesis in *Pelargonium* as it is in peppermint. We were unable to detect pulegone by GC-MS analysis in scan mode. Using a dedicated SIM method for the characteristic ions of pulegone (*m/z* 152, 81, and 67) and SPME adsorption to minimize background, we observed a barely discernible peak at the expected retention time of 16.28 min in *Pelargonium* (Supplementary Fig. S3), but this was below the limit of detection of our analysis. Furthermore, its identity could not be confirmed as (+)−pulegone as the apex of this mass trace did not align with that of the authentic standard. In contrast, (+)-pulegone was readily detectable in peppermint extracts (Supplementary Fig. S3). When we compared this peak in extracts made from similar amounts of fresh tissue from each species, the unknown peak in *Pelargonium* was present at nearly 400-fold lower concentration (<0.3% by peak area) than the confirmed (+)-pulegone in peppermint, making it unlikely that pulegone, if indeed present in *Pelargonium*, plays the same role in *Pelargonium* that it does in peppermint. Moreover, when we made a similar comparison of the peak corresponding to

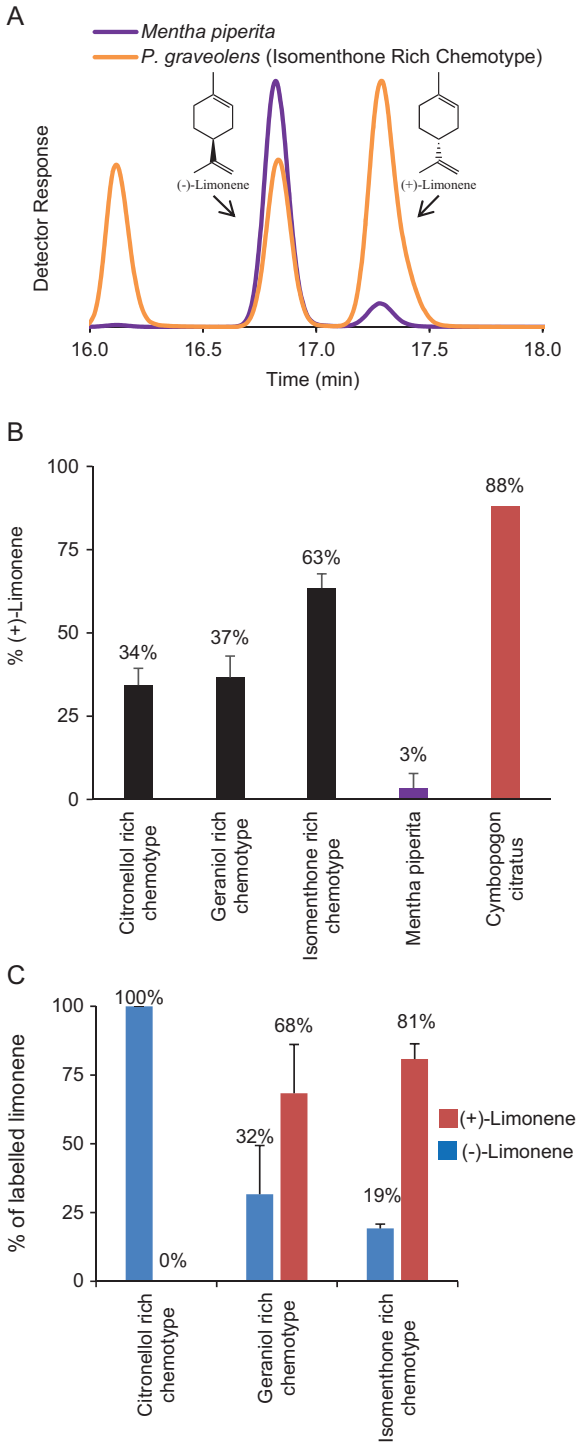

Fig. 7. Stereochemical analysis of ^{13}C label incorporation into limonene enantiomers in *p*-menthane monoterpene-rich and -poor *P. graveolens* chemotypes. (–)-Isomenthone accumulating lines are enriched in a variety of *p*-menthane monoterpenes, including limonene, while (–)-citronellol- and geraniol-rich strains are comparatively depleted in cyclic monoterpenes. (A) (+)-Limonene and (–)-limonene were separated on a β-cyclodex capillary GC column. An extract from peppermint (*M.* × *piperita*), a known producer of mostly (–)-limonene, was included as a reference. (B) Enantiomeric enrichment of limonene enantiomers among *P. graveolens* chemotypes as well as peppermint (*M.* × *piperita*) and lemongrass (*C. citratus*), a known producer of (+)-limonene. (C) Relative incorporation of ^{13}C into (+)- or (–)-limonene during whole plant labeling, as judged by analysis of the molecular ion cluster at *m/z* 136 (M+0) through *m/z* 144 (M+8). Limonene content in the citronellol and geraniol chemotypes is approximately 10-fold lower compared with isomenthone chemotypes. (This figure is available in color at *JXB* online.)

(+)-piperitone in *Pelargonium* and peppermint, the situation was reversed: *Pelargonium* showed 60-fold more (+)-piperitone than peppermint per milligram fresh weight. Furthermore, the (+)-pipertitone pool in *Pelargonium* showed rapid labeling kinetics, confirming it is a rapidly turned over intermediate, while isotope analysis of the putative (+)-pulegone in *Pelargonium* was not possible due to extremely low abundance. Given these observations, we conclude that (+)-pulegone, if present at all in *Pelargonium*, is present at such trace levels that it is highly unlikely it participates in the biosynthesis of *p*-menthane monoterpenes in this species. Furthermore, the rapid labeling kinetics of (+)-piperitone and its significantly higher steady state concentrations led us to conclude that in *Pelargonium*, unlike in peppermint, (+)-piperitone serves as an upstream intermediate to the formation of (−)-isomenthone, while (+)-pulegone does not.

Hierarchical clustering of volatiles in Pelargonium *cultivars highlights the division between* p*-menthane and citronelloid monoterpenoid biosynthesis*

We analysed the complete volatile profiles of several well-known *Pelargonium* hybrids and species along with the representative chemotypes described above to gain further insight into the organization of the two principal monoterpene biosynthetic networks that characterize this genus. In contrast to Fig. 4, this comparison involves more distantly related species. Similar comparisons have been carried out for chemotaxonomic purposes (Lalli *et al.*, 2006) although molecular phylogeny of the chloroplast, mitochondrial, and nuclear genomes may be more accurate (Bakker *et al.*, 2000, 2004). Hierarchical clustering of 132 distinct volatile compounds from 17 *Pelargonium* specimens representing wild species, cultivars, or chemotypes of *P. graveolens* demonstrated clustering that was only weakly consistent with their generally accepted taxonomic relationships (Fig. 8A, B). For instance, the citronellol chemotype grouped closely with *P. radens* due to high levels of (−)-citronellol in both, consistent with Bakker *et al.*, but the isomenthone chemotype of *P. graveolens* grouped closely with *P. tomentosum* due to an abundance of *p*-menthanes in each, despite molecular approaches placing these two species much further apart than *P. graveolens* and *P. radens*.

Despite the lack of conformity between chemotaxonomic approaches and molecular phylogeny, we nonetheless found that inclusion of a wider variety of *Pelargonium* species and cultivars illustrated other likely biosynthetic intermediates associated with each of the two monoterpenoid pathways. For instance, correlation analysis of the 14 most significant features suggests piperitol, piperitone, limonene, menthone, and isomenthone, which all bear a *p*-menthane skeleton, share a common biosynthetic pathway (Fig. 8C). On the other hand, the acyclic citronelloid monoterpenes (geraniol, neral, geraniol, (−)-citronellol, and the formate esters of geraniol and (−)-citronellol) seen in other lines are notably depleted when *p*-menthane skeletal types are abundant. Conversely, citronelloid monoterpenes co-occur strongly and are similarly deficient in *p*-menthane types. This is consistent with the overall division of these two pathways and further supports the

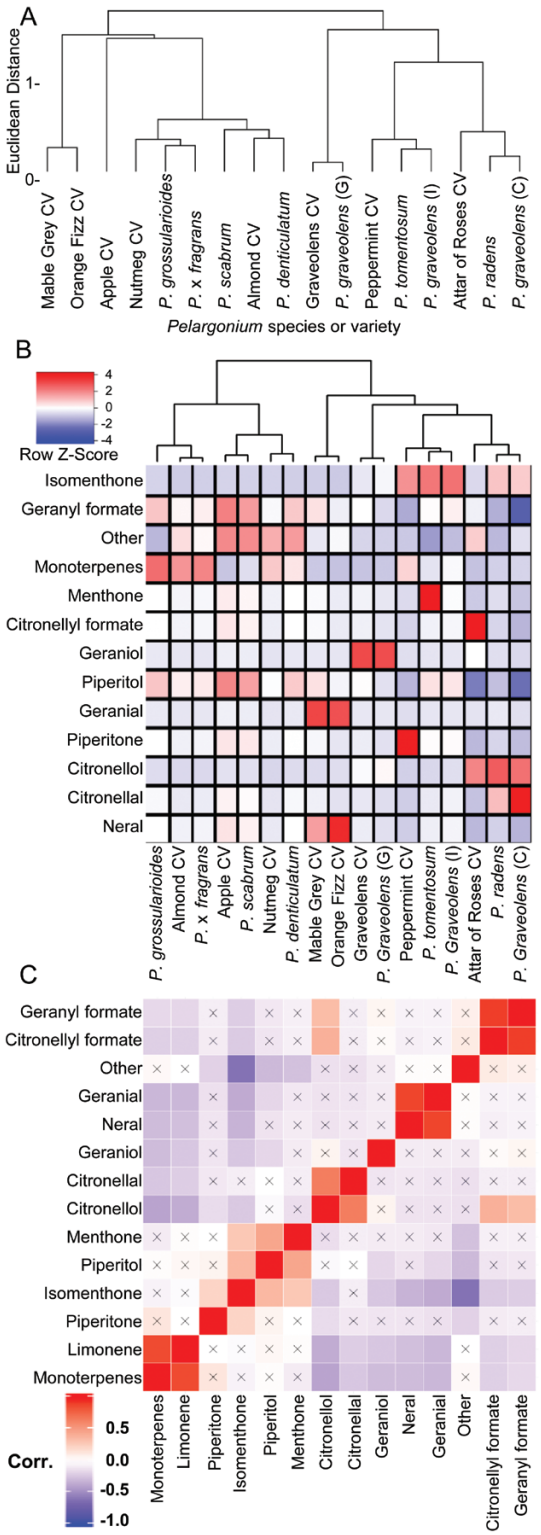

Fig. 8. Hierarchical cluster analysis of *Pelargonium* cultivated varieties and species. (A) Hierarchical clustering of 17 *Pelargonium* varieties including the three *P. graveolens* chemotypes based on volatile profiles consisting of 132 features from untargeted GC-MS analysis. Clustering was performed using the Ward algorithm and separated by Euclidean distance. (B) Heatmap of 14 characteristic volatile features used in the hierarchical clustering of *P. graveolens* lines. (C) corresponding correlation matrix of the same features using 177 total samples across all 17 groups based on their Pearson correlation coefficients. An '×' signifies a lack of statistical significance. The *P.* × *fragrans* used in this study is also known as the 'Old Spice' cultivar. (This figure is available in color at *JXB* online.)

notion that one or the other tends to predominate in a given species or cultivar while examples of comparable proportions of *p*-menthanes and citronelloids, as seen in the 'Graveolens' cultivar, are the exception.

The structure of the monoterpenoid biosynthetic network in P. graveolens *can be partly inferred from isotopic labeling studies*

From these observations, we conclude that monoterpenoid biosynthesis in *P. graveolens*, and likely other members of this genus, can be characterized by variable contributions of two pathways that yield either cyclic *p*-menthane type monoterpenes such as (−)-isomenthone and (+)-menthone or acyclic monoterpene alcohols and their derivatives, described collectively here as citronelloid monoterpenes. The latter command a higher value in fragrance and flavoring industries and are generally more pleasing to the human olfactory palette. Breeders have traditionally selected for *Pelargonium* hybrids enriched in geraniol, citronellol, and nerol and depleted in isomenthone. We initially considered whether these cyclic and acyclic monoterpene groups shared common intermediates, for instance through the cyclization of a non-activated acyclic precursor. Neral and (−)-citronellal (Fig. 1) possess the correct electronic and geometric configurations for direct cyclization into (+)-piperitone and (−)-isomenthone, respectively, via a hydride shift. While unusual, a similar reaction has been reported for a promiscuous squalene-hopene cyclase from the Gram-negative bacterium *Zymomonas mobilis* capable of converting citronellal into isopulegol in bioreactors (Siedenburg *et al.*, 2012). However, our heatmap and correlation data (Fig. 4B, C) clearly show that the *p*-menthane and citronelloid skeletal types are largely mutually exclusive in wild-type lines, a pattern that holds in cultivated hybrids as well (Fig. 8), making a direct connection between these two pathways highly unlikely. Moreover, the strong correlation we observed between flux into (+)-limonene and flux into (−)-isomenthone (Fig. 7), an effect absent in (−)-isomenthone-deficient lines, supports the functional independence of these two pathways with (+)-limonene currently the best candidate for precursor to *p*-menthane monoterpenes in this species.

We further conclude that the glandular trichomes of *P. graveolens* favor *p*-menthane biosynthesis leading to (−)-isomenthone production over citronelloid production in their natural state, an effect likely rooted in the metabolic control of these two pathways. This conclusion is based on the significant levels of measured flux through the *p*-menthane pathway even in geraniol- and (−)-citronellol-specializing lines (Table 1; Supplementary Fig. S2). In contrast, flux towards the citronelloid types in (−)-isomenthone chemotypes was virtually undetectable. The overall magnitude of flux also grossly favored (−)-isomenthone production when the calculated rates of labeling were compared between the main end-products in each of the three chemotypes (1719 pmol ^{13}C mg^{-1} FW h^{-1} (−)-isomenthone in the (−)-isomenthone chemotype versus 218 and 70 pmol ^{13}C mg^{-1} FW h^{-1} (−)-citronellol and geraniol, respectively, in their respective chemotypes). Such a dominant role of the *p*-menthane pathway in determining product

profiles would also be consistent with instances of spontaneous reversion of geraniol-rich cultivars to isomenthone-rich lines (Kulkarni *et al.*, 1998; Gupta *et al.*, 2001; Saxena *et al.*, 2004). The identification of protein targets to overcome this natural tendency towards (−)-isomenthone production would be of value to breeders aiming to maximize geraniol and (−)-citronellol production, as well as their highly valued esters. Similar approaches to improving EO quality in peppermint relied on the identification of the menthofuran synthase gene, whose protein product diverts flux towards the undesirable product (+)-menthofuran (Bertea *et al.*, 2001). Suppression of this transcript enabled a reduction of (+)-menthofuran content and improvement of oil quality (Mahmoud and Croteau, 2003).

The use of volatile profiling to define chemotypes has also been applied to oregano (Thompson *et al.*, 2003), and these chemotypes were central to the elucidation of the biosynthetic pathway of phenolic monoterpenes in this species (Crocoll *et al.*, 2010). The present work identifies future targets for cloning and biochemical characterization and provides a context for understanding the significance of essential oil genes identified to date. Blerot *et al.* (2018) recently characterized four terpene synthases from *P.* × *hybridum*, including the enzyme responsible for the formation of geraniol from GDP, but no enzyme from this genus responsible for its reduction to (−)-citronellol has yet been identified. Indeed, Wüst *et al.* (1999) suggested that *P. graveolens* uses citronellyl diphosphate as a precursor to rose oxide, a high value monoterpene volatile structurally similar to citronellol, and this prenyl diphosphate could potentially serve as the precursor to (−)-citronellol as well. A limonene synthase has similarly not yet been identified from this genus, nor has any other gene related to *p*-menthane metabolism. While molecular, localization, and biochemical data aimed at understanding the metabolic sequence leading to monoterpenoid formation in this species are currently limited, the metabolic data presented here provide a framework for evaluating the physiological relevance of future cloning, expression, and biochemical characterization in this species. Efforts to isolate the corresponding transcripts responsible for the metabolism of monoterpenoid volatiles in this species are currently underway.

Supplementary data

Supplementary data are available at *JXB* online.

Fig. S1. Leaf morphology of representative *P. graveolens* chemotypes.

Fig. S2. Time course labelling of monoterpene volatiles in *P. graveolens* chemotypes identified from a natural population.

Fig. S3. SPME-GC-MS analysis of *p*-menthane volatiles from peppermint and the isomenthone-rich chemotype of *P. graveolens*.

Acknowledgements

This work was supported by a Discovery grant provided by the Natural Sciences and Engineering Research Council (RGPIN-2017-06400, to MP) and by a John Evans Leadership Fund grant from the Canadian Foundation for Innovation (36131, to M P). The authors declare no competing interests.

References

Alberts AW, Chen J, Kuron G, *et al*. 1980. Mevinolin: a highly potent competitive inhibitor of hydroxymethylglutaryl-coenzyme A reductase and a cholesterol-lowering agent. Proceedings of the National Academy of Sciences, USA **77**, 3957–3961.

Andrade P, Manzano D, Ramirez-Estrada K, Caudepon D, Arro M, Ferrer A, Phillips MA. 2018. Nerolidol production in agroinfiltrated tobacco: Impact of protein stability and membrane targeting of strawberry (*Fragraria ananassa*) NEROLIDOL SYNTHASE1. Plant Science **267**, 112–123.

Babu KGD, Kaul VK. 2005. Variation in essential oil composition of rose-scented geranium (*Pelargonium* sp.) distilled by different distillation techniques. Flavour and Fragrance Journal **20**, 222–231.

Bach TJ, Boronat A, Campos N, Ferrer A, Vollack K-U. 1999. Mevalonate biosynthesis in plants. Critical Reviews in Biochemistry and Molecular Biology **34**, 107–122.

Bakker FT, Culham A, Hettiarachi P, Touloumenidou T, Gibby M. 2004. Phylogeny of *Pelargonium* (Geraniaceae) based on DNA sequences from three genomes. Taxon **53**, 17–31.

Bakker FT, Culham A, Pankhurst CE, Gibby M. 2000. Mitochondrial and chloroplast DNA-based phylogeny of *Pelargonium* (Geraniaceae). American Journal of Botany **87**, 727–734.

Balcke GU, Bennewitz S, Bergau N, Athmer B, Henning A, Majovsky P, Jiménez-Gómez JM, Hoehenwarter W, Tissier A. 2017. Multi-omics of tomato glandular trichomes reveals distinct features of central carbon metabolism supporting high productivity of specialized metabolites. The Plant Cell **29**, 960–983.

Baldin ELL, Aguiar GP, Fanela TLM, Soares MCE, Groppo M, Crotti AEM. 2015. Bioactivity of *Pelargonium graveolens* essential oil and related monoterpenoids against sweet potato whitefly, *Bemisia tabaci* biotype B. Journal of Pest Science **88**, 191–199.

Banerjee A, Sharkey TD. 2014. Methylerythritol 4-phosphate (MEP) pathway metabolic regulation. Natural Product Reports **31**, 1043–1055.

Bertea CM, Schalk M, Karp F, Maffei M, Croteau R. 2001. Demonstration that menthofuran synthase of mint (*Mentha*) is a cytochrome P450 monooxygenase: cloning, functional expression, and characterization of the responsible gene. Archives of Biochemistry and Biophysics **390**, 279–286.

Blerot B, Baudino S, Prunier C, Demarne F, Toulemonde B, Caissard JC. 2016. Botany, agronomy and biotechnology of *Pelargonium* used for essential oil production. Phytochemistry Reviews **15**, 935–960.

Blerot B, Martinelli L, Prunier C, *et al*. 2018. Functional analysis of four terpene synthases in rose-scented Pelargonium cultivars (*Pelargonium* × *hybridum*) and evolution of scent in the *Pelargonium* genus. Frontiers in Plant Science **9**, 1435.

Booth JK, Page JE, Bohlmann J. 2017. Terpene synthases from *Cannabis sativa*. PLoS One **12**, e0173911.

Boukhris M, Ben Nasri-Ayachi M, Mezghani I, Bouaziz M, Boukhris M, Sayadi S. 2013*a*. Trichomes morphology, structure and essential oils of *Pelargonium graveolens* L'Hér. (Geraniaceae). Industrial Crops and Products **50**, 604–610.

Boukhris M, Bouaziz M, Feki I, Jemai H, El Feki A, Sayadi S. 2012. Hypoglycemic and antioxidant effects of leaf essential oil of *Pelargonium graveolens* L'Hér. in alloxan induced diabetic rats. Lipids in Health and Disease **11**, 81.

Boukhris M, Hadrich F, Chtourou H, Dhouib A, Bouaziz M, Sayadi S. 2015. Chemical composition, biological activities and DNA damage protective effect of *Pelargonium graveolens* L'Hér. essential oils at different phenological stages. Industrial Crops and Products **74**, 600–606.

Boukhris M, Simmonds MS, Sayadi S, Bouaziz M. 2013*b*. Chemical composition and biological activities of polar extracts and essential oil of rose-scented geranium, *Pelargonium graveolens*. Phytotherapy Research **27**, 1206–1213.

Champagne A, Boutry M. 2017. A comprehensive proteome map of glandular trichomes of hop (*Humulus lupulus* L.) female cones: identification of

biosynthetic pathways of the major terpenoid-related compounds and possible transport proteins. Proteomics **17**, 1600411.

Chen W, Viljoen A. 2010. Geraniol—a review of a commercially important fragrance material. South African Journal of Botany **76**, 643–651.

Chong J, Soufan O, Li C, Caraus I, Li S, Bourque G, Wishart DS, Xia J. 2018. MetaboAnalyst 4.0: towards more transparent and integrative metabolomics analysis. Nucleic Acids Research **46**, W486–W494.

Crocoll C, Asbach J, Novak J, Gershenzon J, Degenhardt J. 2010. Terpene synthases of oregano (*Origanum vulgare* L.) and their roles in the pathway and regulation of terpene biosynthesis. Plant Molecular Biology **73**, 587–603.

Croteau RB, Davis EM, Ringer KL, Wildung MR. 2005. (–)-Menthol biosynthesis and molecular genetics. Naturwissenschaften **92**, 562.

Delwiche C, Sharkey T. 1993. Rapid appearance of ^{13}C in biogenic isoprene when $^{13}CO_2$ is fed to intact leaves. Plant, Cell & Environment **16**, 587–591.

Demarne F, Van der Walt J. 1989. Origin of the rose-scented *Pelargonium* cultivar grown on Réunion Island. South African Journal of Botany **55**, 184–191.

Doimo L, Mackay DC, Rintoul GB, D'Arcy BR, Fletcher RJ. 1999. Citronellol: geraniol ratios and temperature in geranium (Pelargonium hybrid). Journal of Horticultural Science and Biotechnology **74**, 528–530.

Frank A, Groll M. 2017. The methylerythritol phosphate pathway to isoprenoids. Chemical Reviews **117**, 5675–5703.

Galili T. 2015. dendextend: an R package for visualizing, adjusting and comparing trees of hierarchical clustering. Bioinformatics **31**, 3718–3720.

Galili T, O'callaghan A, Sidi J, Sievert C. 2017. heatmaply: an R package for creating interactive cluster heatmaps for online publishing. Bioinformatics **34**, 1600–1602.

Gershenzon J, Dudareva N. 2007. The function of terpene natural products in the natural world. Nature Chemical Biology **3**, 408.

Ghirardo A, Wright LP, Bi Z, Rosenkranz M, Pulido P, Rodríguez-Concepción M, Niinemets Ü, Brüggemann N, Gershenzon J, Schnitzler J-P. 2014. Metabolic flux analysis of plastidic isoprenoid biosynthesis in poplar leaves emitting and non-emitting isoprene. Plant Physiology **165**, 137–151.

Gupta R, Mallavarapu G, Banerjee S, Kumar S. 2001. Characteristics of an isomenthone-rich somaclonal mutant isolated in a geraniol-rich rose-scented geranium accession of *Pelargonium graveolens*. Flavour and Fragrance Journal **16**, 319–324.

Hallahan DL. 2000. Monoterpenoid biosynthesis in glandular trichomes of labiate plants. Advances in Botanical Research **31**, 77–120.

Hedden P, Thomas S.G. 2012. Gibberellin biosynthesis and its regulation. Biochemical Journal **444**, 11.

Hoeffler JF, Hemmerlin A, Grosdemange-Billiard C, Bach TJ, Rohmer M. 2002. Isoprenoid biosynthesis in higher plants and in *Escherichia coli*: on the branching in the methylerythritol phosphate pathway and the independent biosynthesis of isopentenyl diphosphate and dimethylallyl diphosphate. Biochemical Journal **366**, 573–583.

Houshyani B, Assareh M, Busquets A, Ferrer A, Bouwmeester HJ, Kappers IF. 2013. Three-step pathway engineering results in more incidence rate and higher emission of nerolidol and improved attraction of *Diadegma semiclausum*. Metabolic Engineering **15**, 88–97.

Jain N, Aggarwal K, Syamasundar K, Srivastava S, Kumar S. 2001. Essential oil composition of geranium (*Pelargonium* sp.) from the plains of Northern India. Flavour and Fragrance Journal **16**, 44–46.

Jeon J, Lee C, Lee H. 2009. Food protective effect of geraniol and its congeners against stored food mites. Journal of Food Protection **72**, 1468–1471.

Karami A, Khorshidi R, Jowkar A. 2015. Diurnal changes in the volatile oil compounds of rose-scented geranium (*Pelargonium graveolens*). Analytical Chemistry Letters **5**, 103–108.

Karl T, Fall R, Rosenstiel T, Prazeller P, Larsen B, Seufert G, Lindinger W. 2002. On-line analysis of the $^{13}CO_2$ labeling of leaf isoprene suggests multiple subcellular origins of isoprene precursors. Planta **215**, 894–905.

Kim S, Schlicke H, Van Ree K, Karvonen K, Subramaniam A, Richter A, Grimm B, Braam J. 2013. *Arabidopsis* chlorophyll biosynthesis: an essential balance between the methylerythritol phosphate and tetrapyrrole pathways. The Plant Cell **25**, 4984–4993.

Kulkarni R, Mallavarapu G, Baskaran K, Ramesh S, Kumar S. 1998. Composition of the essential oils of two isomenthone-rich variants of geranium (*Pelargonium* sp.). Flavour and Fragrance Journal **13**, 389–392.

Lalli JYY, Viljoen AM, Baser KHC, Demirci B, Oezek T. 2006. The essential oil composition and chemotaxonomical appraisal of South African Pelargoniums (Geraniaceae). Journal of Essential Oil Research **18**, 89–105.

Lange BM. 2015. Biosynthesis and biotechnology of high-value P-menthane monoterpenes, including menthol, carvone, and limonene. Advances in Biochemical Engineering/Biotechnology **148**, 319–353.

Lis-Balchin M, Buchbauer G, Hirtenlehner T, Resch M. 1998. Antimicrobial activity of *Pelargonium* essential oils added to a quiche filling as a model food system. Letters in Applied Microbiology **27**, 207–210.

Lis-Balchin M, Deans SG. 1997. Bioactivity of selected plant essential oils against *Listeria monocytogenes*. Journal of Applied Microbiology **82**, 759–762.

Lis-Balchin M, Steyrl H, Krenn E. 2003. The comparative effect of novel *Pelargonium* essential oils and their corresponding hydrosols as antimicrobial agents in a model food system. Phytotherapy Research **17**, 60–65.

Liu M, Lu S. 2016. Plastoquinone and ubiquinone in plants: biosynthesis, physiological function and metabolic engineering. Frontiers in Plant Science **7**, 1898.

Loehrlein M, Craig R. 2000. Floral ontogeny of *Pelargonium* × *domesticum*. Journal of the American Society for Horticultural Science **125**, 36–40.

Loehrlein MM, Craig R. 2001. History and culture of regal pelargonium. HortTechnology **11**, 289–296.

Loreto F, Ciccioli P, Brancaleoni E, Cecinato A, Frattoni M, Sharkey TD. 1996. Different sources of reduced carbon contribute to form three classes of terpenoid emitted by *Quercus ilex* L. leaves. Proceedings of the National Academy of Sciences, USA **93**, 9966–9969.

Loreto F, Pinelli P, Brancaleoni E, Ciccioli P. 2004. ^{13}C labeling reveals chloroplastic and extrachloroplastic pools of dimethylallyl pyrophosphate and their contribution to isoprene formation. Plant Physiology **135**, 1903–1907.

Mahmoud SS, Croteau RB. 2003. Menthofuran regulates essential oil biosynthesis in peppermint by controlling a downstream monoterpene reductase. Proceedings of the National Academy of Sciences, USA **100**, 14481–14486.

Matsue Y, Mizuno H, Tomita T, Asami T, Nishiyama M, Kuzuyama T. 2006. The herbicide ketoclomazone inhibits 1-deoxy-D-xylulose 5-phosphate synthase in the 2-*C*-methyl-D-erythritol 4-phosphate pathway and shows antibacterial activity against *Haemophilus influenzae*. Journal of Antibiotics **63**, 583–588.

McCaskill D, Gershenzon J, Croteau R. 1992. Morphology and monoterpene biosynthetic capabilities of secretory cell clusters isolated from glandular trichomes of peppermint (*Mentha piperita* L.). Planta **187**, 445–454.

Nadjib Boukhatem M, Kameli A, Amine Ferhat M, Saidi F, Mekarnia M. 2013. Rose geranium essential oil as a source of new and safe anti-inflammatory drugs. Libyan Journal of Medicine **8**, 22520.

Nambara E, Marion-Poll A. 2005. Abscisic acid biosynthesis and catabolism. Annual Review of Plant Biology **56**, 165–185.

Pare PW, Tumlinson JH. 1997. De novo biosynthesis of volatiles induced by insect herbivory in cotton plants. Plant Physiology **114**, 1161.

Phillips MA, León P, Boronat A, Rodríguez-Concepción M. 2008. The plastidial MEP pathway: unified nomenclature and resources. Trends in Plant Science **13**, 619–623.

Phillips MA, Savage TJ, Croteau R. 1999. Monoterpene synthases of loblolly pine (*Pinus taeda*) produce pinene isomers and enantiomers. Archives of Biochemistry and Biophysics **372**, 197–204.

Phillips MA, Wildung MR, Williams DC, Hyatt DC, Croteau R. 2003. cDNA isolation, functional expression, and characterization of (+)-α-pinene synthase and (–)-α-pinene synthase from loblolly pine (*Pinus taeda*): stereocontrol in pinene biosynthesis. Archives of Biochemistry and Biophysics **411**, 267–276.

Rajeswara Rao BR. 2009. Chemical composition and uses of Indian rose-scented geranium (*Pelargonium* species) essential oil – a review. Journal of Essential Oil-Bearing Plants **12**, 381–394.

Rajeswara Rao BR, Kaul PN, Mallavarapu GR, Ramesh S. 1996. Effect of seasonal climatic changes on biomass yield and terpenoid composition

of rose-scented geranium (*Pelargonium* species). Biochemical Systematics and Ecology **24**, 627–635.

Ravid U, Putievsky E, Katzir I. 1994. Chiral GC analysis of menthone and isomenthone with high enantiomeric purities in laboratory-made and commercial essential oils. Flavour and Fragrance Journal **9**, 139–142.

Ruiz-Sola MÁ, Rodríguez-Concepción M. 2012. Carotenoid biosynthesis in Arabidopsis: a colorful pathway. The Arabidopsis Book **10**, e0158.

Sakakibara H. 2006. Cytokinins: activity, biosynthesis, and translocation. Annual Review of Plant Biology **57**, 431–449.

Saxena G, Banerjee S, Gupta R, **Laiq-ur-Rahman**, **Tyagi BR, Kumar S, Mallavarapu GR, Ramesh S.** 2004. Composition of the essential oil of a new isomenthone-rich variant of geranium obtained from geraniol-rich cultivar of *Pelargonium* species. Journal of Essential Oil Research **16**, 85–88.

Seo S-M, Kim J, Lee S-G, Shin C-H, Shin S-C, Park I-K. 2009. Fumigant antitermitic activity of plant essential oils and components from ajowan (*Trachyspermum ammi*), allspice (*Pimenta dioica*), caraway (*Carum carvi*), dill (*Anethum graveolens*), geranium (*Pelargonium graveolens*), and litsea (*Litsea cubeba*) ocils against Japanese termite (*Reticulitermes speratus* Kolbe). Journal of Agricultural and Food Chemistry **57**, 6596–6602.

Shellie RA, Marriott PJ. 2003. Comprehensive two-dimensional gas chromatography-mass spectrometry analysis of *Pelargonium graveolens* essential oil using rapid scanning quadrupole mass spectrometry. Analyst **128**, 879–883.

Siedenburg G, Jendrossek D, Breuer M, Juhl B, Pleiss J, Seitz M, Klebensberger J, Hauer B. 2012. Activation-independent cyclization of monoterpenoids. Applied and Environmental Microbiology **78**, 1055–1062.

Thompson JD, Chalchat J-C, Michet A, Linhart YB, Ehlers B. 2003. Qualitative and quantitative variation in monoterpene co-occurrence and composition in the essential oil of *Thymus vulgaris* chemotypes. Journal of Chemical Ecology **29**, 859–880.

Tissier A, Morgan JA, Dudareva N. 2017. Plant volatiles: going 'in' but not 'out' of trichome cavities. Trends in Plant Science **22**, 930–938.

Tucker AO, Debaggio T. 2009. The encyclopedia of herbs. Portland, OR, USA: Timber Press.

Turner G, Gershenzon J, Nielson EE, Froehlich JE, Croteau R. 1999. Limonene synthase, the enzyme responsible for monoterpene biosynthesis in peppermint, is localized to leucoplasts of oil gland secretory cells. Plant Physiology **120**, 879–886.

Verma RS, Rahman Lu, Verma RK, Chauhan A, Singh A. 2013. Essential oil composition of *Pelargonium graveolens* L'Her ex Ait. cultivars harvested in different seasons. Journal of Essential Oil Research **25**, 372–379.

Wang M, Chittiboyina AG, Avonto C, Parcher JF, Khan IA. 2014. Comparison of current chemical and stereochemical tests for the identification and differentiation of *Pelargonium graveolens* L'Hér. (Geraniaceae) essential oils: analytical data for (–)-(1*S*,4*R*,5*S*)-guaia-6,9-diene and (–)-(7*R*,10*S*)-10-epi-γ-eudesmol. Records of Natural Products **8**, 360–372.

Wickham H. 2016. ggplot2: Elegant graphics for data analysis. New York: Springer.

Wüst M, Beck T, Mosandl A. 1999. Conversion of citronellyl diphosphate and citronellyl β-D-glucoside into rose oxide by *Pelargonium graveolens*. Journal of Agricultural and Food Chemistry **47**, 1668–1672.

Xia J, Sinelnikov IV, Han B, Wishart DS. 2015. MetaboAnalyst 3.0—making metabolomics more meaningful. Nucleic Acids Research **43**, W251–W257.